
Experimental early crystallization of K-feldspar in granitic systems. Implications on the origin of magmatic fabrics in granitic rocks

J. DÍAZ-ALVARADO¹

¹Departamento de Geología. Universidad de Atacama
Copayapu 485, Copiapó, Chile. E-mail: juan.diaza@uda.cl

ABSTRACT

One of the most outstanding characteristics of some granodioritic to granitic rocks is the presence of K-feldspar megacrysts. For instance, granodiorites and monzogranites of the Spanish Central System batholith present variable amounts of large (up to 10cm in length) euhedral K-feldspar crystals. The porphyritic textures, the euhedral shape, the alignment of plagioclase and biotite inclusions and the magmatic fabrics point to a magmatic origin for these megacrysts.

This work presents a phase equilibria study in a high-K₂O granodioritic system. A series of experiments were conducted with a granodioritic composition (GEMbiot) to study the crystallization sequence at the emplacement conditions in the Gredos massif, *i.e.* 4 H₂O wt.% and 0.4GPa. Experimental results show that orthopyroxene is the liquidus phase at 1010°C, which reacts with the H₂O-rich melt to stabilize biotite between 980 and 940°C. Plagioclase crystallizes at around 910°C, and K-feldspar crystallizes in the matrix between 750 and 700°C when the crystal fraction is around 0.5. However, at 850°C, a pelite-doped experiment shows euhedral K-feldspar (\approx 5vol%) in both the reactive xenolith domain together with cordierite and the granodioritic domain, where the K₂O wt.% rose from 4.5 in the normal experiment to 5.9 in the doped experiment. These results suggest that the bulk-assimilation process promotes the bulk and heterogeneous K₂O enrichment in a huge granodioritic magma volume, which triggers an early crystallization of K-feldspar megacrysts. Because of this early crystallization of the megacrysts, the magmatic foliations defined by K-feldspar megacrysts are formed during and after the emplacement processes and are highly influenced by tectonic kinematics.

KEYWORDS | K-feldspar megacrysts. Experimental petrology. Granodiorites. Magmatic fabrics. Spanish Central System batholith.

INTRODUCTION

K-feldspar megacrysts are a characteristic feature in some calc-alkaline granodioritic to granitic magmatic suites of large composite batholiths (Weinberg *et al.*, 2001; Moore and Sisson, 2008; Farina *et al.*, 2010; 2012). The origin of K-feldspar megacrysts is still controversial and essential to understand the formation of magmatic structures by the rotation of rigid particles (crystals) in a viscous environment (melt). Evidences are argued in favour and against an early phenocrystic origin of these crystals:

magmatic fabrics, accumulative textures, cross-cutting relations with mineral layers or veins, simple twinning, plagioclase and biotite inclusion alignment, Ca content in megacrysts, Ba zoning, Zr-in-titanite temperatures, the presence of K-feldspar megacrysts in volcanic rocks, enclaves and dikes, experimental crystallization sequences or textural coarsening (Vernon and Paterson, 2008; Johnson and Glazner, 2010; Glazner and Johnson, 2013). K-feldspar megacrysts are almost absent in volcanic dacitic rocks, which are the volcanic equivalents to the megacrystic rocks. This is evidenced in favour of the late crystallization

of megacrysts. Then, temperature cycling determines the coarsening of K-feldspar in megacrystic granites. Heat and time requirements to support this process are supplied by water-rich fluids associated with incremental emplacement (Johnson and Glazner, 2010; Glazner and Johnson, 2013). On the contrary, magmatic fabrics defined by megacrysts and some textural characteristics (internal zonation, inclusion alignment) support the interpretation that K-feldspar megacrysts grow to large sizes early in magma history, while the simultaneously crystallizing quartz and feldspar grains that overgrow irregular megacrysts are interpreted as due to later processes after the growth of euhedral megacrysts (Vernon and Paterson, 2008). Other evidences as the presence of K-feldspar crystals in dioritic enclaves or the relation between megacrysts, schlieren and other magmatic structures remain enigmatic in granitic plutons.

The study of magmatic fabrics in granites, originated by interaction of melt, crystals and a gas phase (London, 2009; Vignerresse, 2014), uses solid particles like K-feldspar megacrysts, whose order of appearance needs to be tightly constrained in the crystallization sequence. The studies of phase relations in the haplogranite system at different pressures ($\text{NaAlSi}_3\text{O}_8$ - KAlSi_3O_8 - SiO_2 - H_2O) began the experimental knowledge of granitic systems (Tuttle and Bowen, 1958; Luth *et al.*, 1964; Peters *et al.*, 1966; Scarfe *et al.*, 1966; Lindsley, 1967; Boettcher and Wyllie, 1969; Lambert *et al.*, 1969; Merrill *et al.*, 1970; Kim and Burley, 1971). Luth (1969), Steiner (1970) and Steiner *et al.* (1975) first studied water-undersaturated systems and, therefore, the role of H_2O in the crystallization process. Besides, the solubility of the volatile phases was also experimentally studied (Burnham *et al.*, 1962; Maaløe and Wyllie, 1975; Wyllie, 1979; Thomas, 2000), and additional components ($\text{NaAlSi}_3\text{O}_8$ - KAlSi_3O_8 - $\text{CaAl}_2\text{Si}_2\text{O}_8$ - SiO_2 - H_2O) were instead considered (Piwinski and Wyllie, 1968, 1970; James and Hamilton, 1969; Whitney, 1975; Holtz *et al.*, 2001).

Despite the relevance of precursory experimental studies, they reproduce only partially the phase relations in the granodioritic system (*e.g.* Naney, 1983). Granodiorites and tonalites are defined, in terms of major elements, as high-silica rocks (70-63 wt.% SiO_2) that show FeO, MgO and CaO contents ranging from 2-5, 1-3 and 1.5-5 wt.% respectively (Castro, 2013). Mineral assemblages are dominated by calcic plagioclase, hornblende and biotite as mafic minerals, with K-feldspar and quartz usually present in the matrix. Ca, Mg, Fe and K are then responsible for the most frequently observed variations in granodioritic magmas (Castro, 2013). Experimental phase equilibria of ferromagnesian minerals in granitic systems have been studied by Naney (1983), who established the experimental crystallization sequence of a granodioritic magma with

various initial H_2O contents at different pressure conditions. Water content, pressure and temperature determine the crystallization order and the stability of ferromagnesian phases (orthopyroxene, hornblende and biotite) (Luth, 1976; Naney, 1983), whose solubility increase with water content and temperature, and decrease with pressure (Johannes and Holtz, 1996; Patiño Douce, 1996).

In this study, experimental phase equilibria have been determined for bulk compositions similar to those of granites rich in K-feldspar megacrysts (*e.g.* Piwinski, 1968; Whitney, 1988; Johnson and Rutherford, 1989). The results of those experiments suggest that K-feldspar is the last phase to crystallize when crystal content in experimental magmas are over the rheologic threshold of $\approx 50\%$ crystals. Thermodynamic calculations on the crystallization of granitic magmas are in agreement with experimental results and have also shown that K-feldspar is a late crystallization phase (García-Arias and Stevens, 2017). In the case of the Central System batholith, K-feldspar megacrysts are present in most of the granodioritic and monzogranitic facies of the exposed batholith (*e.g.* Díaz-Alvarado *et al.*, 2011, 2012). The simulations of the experimental crystallization sequence are presented here to constrain the experimental conditions for crystallization of K-feldspar in high- K_2O granodiorites, which are compared with the phase and field relations observed in the granodiorites and monzogranites of the Gredos massif. Furthermore, the contribution of metapelitic host-rocks is simulated experimentally with significant results to decipher the early or late origin of K-feldspar megacrysts in granitic magmas, which is essential to assign a magmatic or a sub-solidus origin to the K-feldspar fabrics observed in megacrystic granites.

GEOLOGICAL SETTING OF THE CENTRAL SYSTEM BATHOLITH

The Central System batholith constitutes an almost continuous granite exposure in the Central Iberian Zone of the Iberian Massif (Fig. 1A). Granitic rocks of granodiorite to monzogranite composition constitute more than 90 vol% of the intrusive rocks. Minor amounts of more basic rocks ranging from gabbro to Qtz-diorite are present everywhere in the batholith. In general, all plutonic rocks from gabbros to granodiorites form a typical K-rich calc-alkaline association (Moreno-Ventas *et al.*, 1995) and they belong to the large group of intrusives cataloged as “granodiorites” or “calc-alkaline series granitoids” in regional syntheses and classifications of the Paleozoic magmatism of Iberia (Capdevila *et al.*, 1973; Castro *et al.*, 2002).

In the Gredos massif (Fig. 1A; B), the general structure of the Central System batholith is that of a layered intrusive

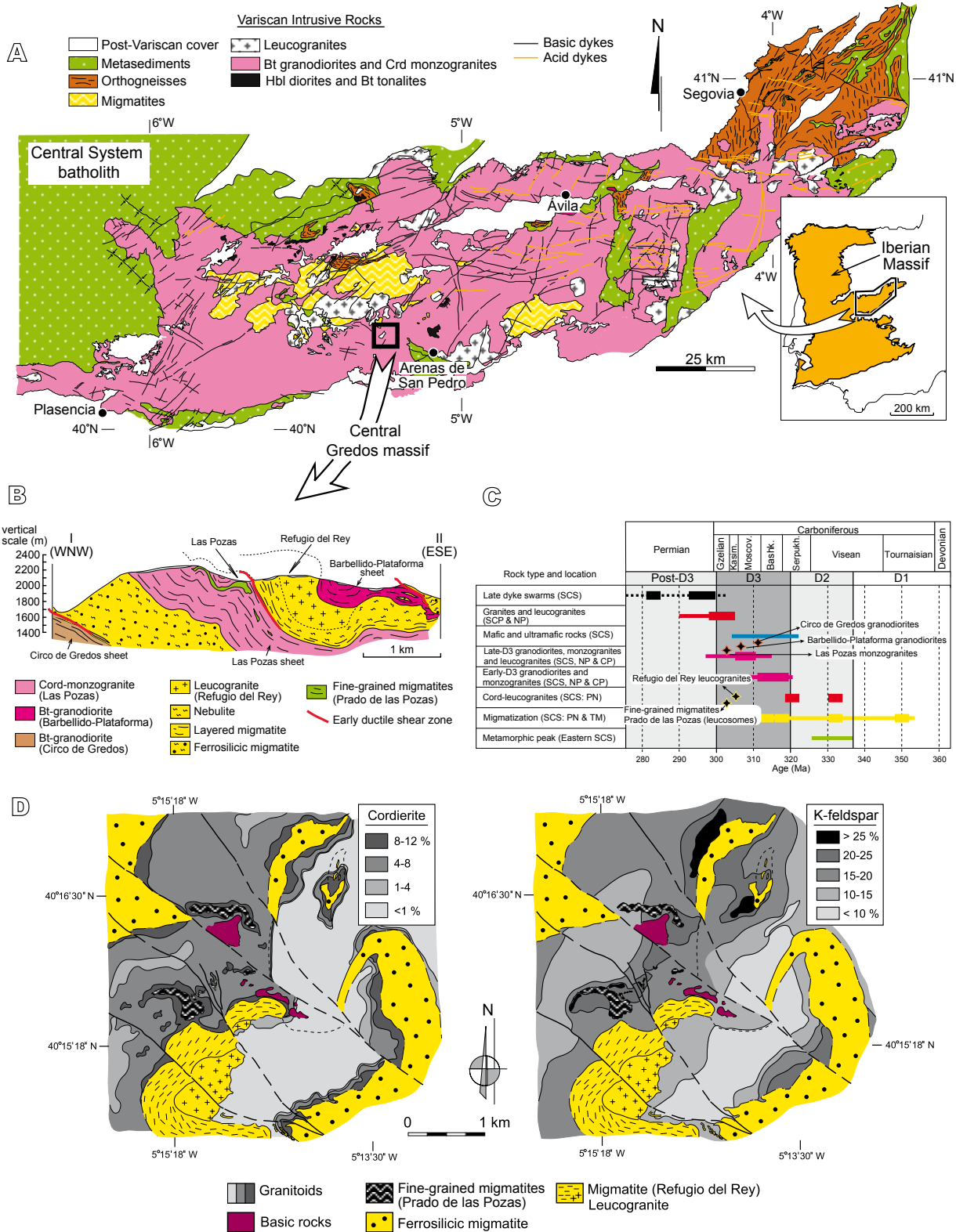


FIGURE 1. Geological setting and main structural, geochronological and petrological characteristics of the Gredos massif in the Central System batholith. A) Geological map of the Spanish Central System batholith. B) Detailed geological cross-section of the studied zone. C) Diagram showing the age variation and time relations of tectonic and metamorphic processes and granitoid generation and intrusion in the Central System batholith and nearby regions of the Central Iberian Zone (Iberian Massif), modified from Díaz-Alvarado *et al.* (2013). SCS: Spanish Central System; NP: Northern Portugal; CP: Central Portugal; PN: Peña Negra; TM: Tormes massif. D1 to D3: Variscan deformation phases. D) Isocontour maps representing the volume fractions of cordierite and K-feldspar in the granitoids of the Gredos massif (Díaz-Alvarado *et al.*, 2011).

complex, with distinct magma batches that successively intruded a migmatitic crust, derived from pelitic and semipelitic metasediments that form part of a several km thick Neo-Proterozoic turbiditic series (Rodríguez Alonso *et al.*, 2004) and Ordovician ferrosilicic metavolcanics (Parga-Pondal *et al.*, 1964; Fernández *et al.*, 2008; Castro *et al.*, 2009; Díaz-Alvarado *et al.*, 2016). The emplacement of these tabular magma bodies profited from large extensional shear zones affecting the migmatitic host-rocks (Fig. 1B). Detailed geochronological and structural studies show that the main period of magma intrusion took place between 312.6 ± 2.8 Ma and 303.5 ± 2.8 Ma for the bottom (Circo de Gredos), upper (Barbellido-Plataforma) and middle (Las Pozas) granitic sheets in the inner Gredos massif, contemporary with the extensional and transtensional episodes of the regional Late Paleozoic D3 deformation phase (see Díaz-Alvarado *et al.*, 2013 and references therein) (Fig. 1C). Mainly in areas adjacent to the metasedimentary host-rocks, intrusive granitoids present prominent heterogeneities related to variable percentages of euhedral cordierite, between 1 and 12 vol% in Crd-monzogranites, and K-feldspar megacrysts, with values over 25 vol% in monzogranitic magma batches around the metasediment bodies (Fig. 1D). These differences have been interpreted as caused by the interaction (including mainly assimilation processes) of magma and host-rocks (Díaz-Alvarado *et al.*, 2011).

FIELD AND PHASE RELATIONS OF GRANODIORITES AND MONZOGRANITES IN THE GREDOS MASSIF

Large euhedral K-feldspar crystals show prominent apparent constriction and flattening magmatic fabrics in coarse-grained, mesocratic monzogranites and granodiorites of the Gredos massif (Díaz-Alvarado *et al.*, 2012), composed of quartz, plagioclase (An₆₅₋₃₂), K-feldspar and biotite (cordierite is present in Crd-monzogranites). These granites (*s.l.*) are commonly porphyritic with large K-feldspar phenocrysts (up to 10cm length) (Fig. 2A) heterogeneously distributed in bands and irregular patches (Fig. 2B). Megacrysts show euhedral biotite and zoned plagioclase inclusions mostly aligned in concentric bands (Fig. 2C). They present both sharp contacts or they extend into the groundmass and show magmatic overgrowths with quartz and plagioclase.

Magmatic foliations were affected by two generations of folds (Fig. 2D), which created a complex fold interference pattern (Díaz-Alvarado *et al.*, 2012). Magma-magma contacts are observed between magma batches, which can be distinguished due to the variable content in K-feldspar megacrysts (Fig. 2B), among other features. Solid-state structures are scarce and mostly related with NW-SE late shear zones. Crystallization and sequential emplacement of

the intrusive bodies proceeded simultaneously according to the relations observed in the magma and host-rocks contacts. K-feldspar crystals of variable size appear in the intrusive layers and their long axes tend to run parallel with host-rock contacts and migmatitic structures (Fig. 2E; F). These observations together with geochronological data (Fig. 1C) suggest that melt generation and segregation in the migmatitic host-rocks were coeval with the intrusion of granodioritic magmas in the study area, and a strong deformational and geochemical interaction between the intrusive magmas and the migmatitic crust took place during the emplacement period (Fig. 2).

EXPERIMENTAL STRATEGY, STARTING MATERIALS AND PROCEDURES

Strategy

A set of experiments was carried out in order to constrain the crystallization sequence in a K-rich granodioritic system, with the aim of simulating the phase relations observed in the calc-alkaline granodiorites and monzogranites of the Gredos massif. The K-feldspar megacrysts and euhedral Crd crystals observed in some granitic facies of the Central System batholith are not predicted by previous experimental studies in granite to granodiorite systems (*e.g.* Maaløe and Wyllie, 1975; Naney, 1983; Johnson and Rutherford, 1989), hence it is necessary to study the significance of high-potassium contents in granodioritic magmas.

Experiments, phase relations and field evidences point out that most granodioritic magmas are water-undersaturated during a wide temperature range of their cooling history (Luth, 1969; Naney, 1983; Castro, 2013 and references therein). Initial conditions were fixed assuming that calc-alkaline granitoids crystallized from strongly undersaturated magmas, with water contents bracketed between a minimum represented by the water coordinated in hydrous minerals (*ca.* 1 wt.% of H₂O) and a maximum corresponding to the saturation of the system at the pressure of emplacement (0.4GPa according to *e.g.* Díaz-Alvarado *et al.*, 2011), *i.e.* 6 wt.% of H₂O according to the Burnham (1979) saturation model.

Starting materials

The compositions of the starting materials used in the experiments are shown in Table 1. A granodioritic synthetic glass (SG-GEMbiot) was designed to reproduce the composition of biotitic granitoids with microgranular enclaves (GEMbiot) determined by Moreno-Ventas Bravo (1991) in the Gredos massif. This composition is representative of a suite of biotite-bearing granodioritic

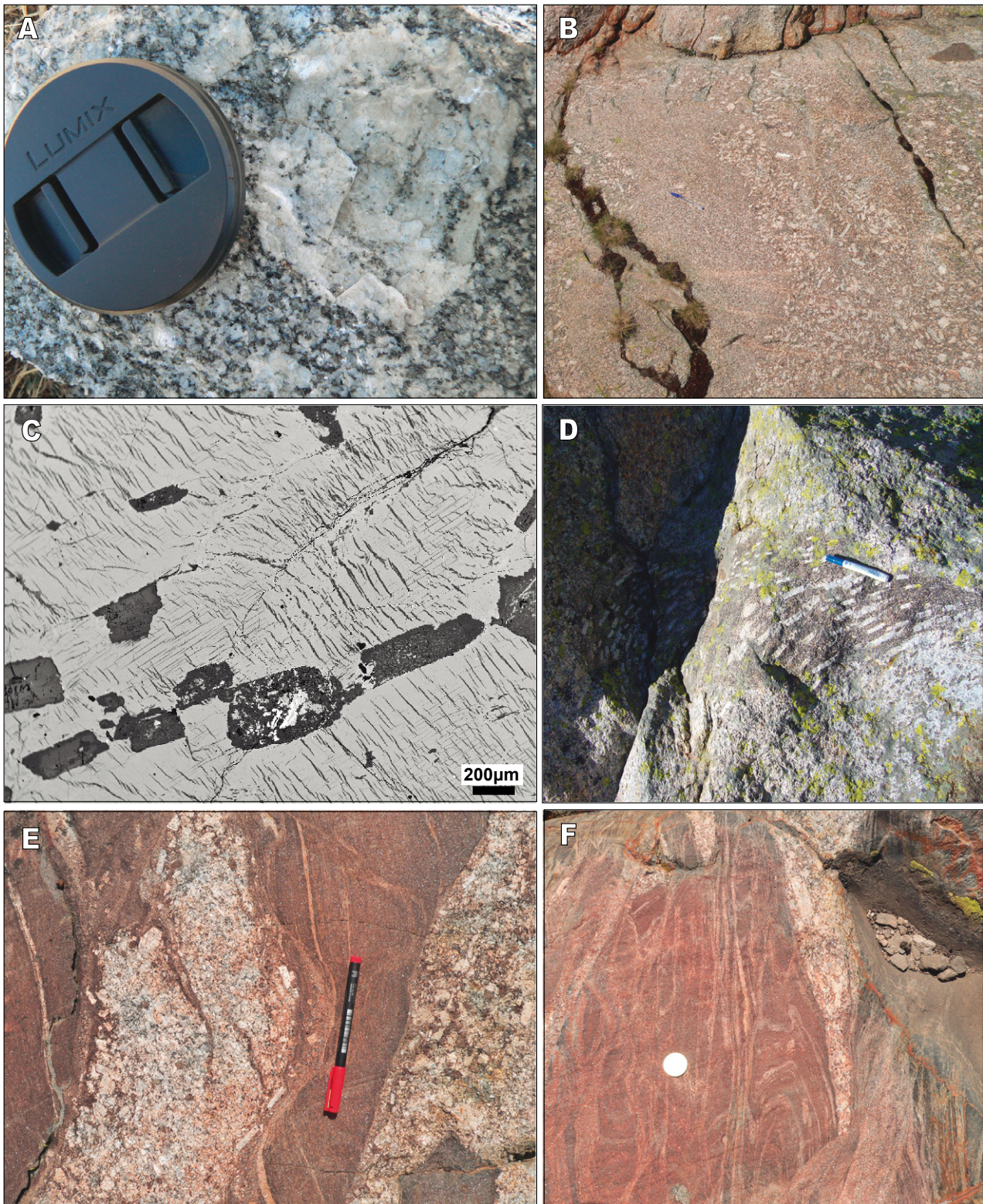


FIGURE 2. Field photographs of the Gredos massif. A) (001) section of a K-feldspar megacrystal showing two inner concentric biotite+plagioclase alignments that separate three growing stages of the megacryst. B) Sharp magma-magma lobate contacts between the different granitic facies in the proximity of the host metasediments. They are mainly recognizable by the K-feldspar megacrystals content. C) BSE image of a K-feldspar megacrystal showing the euhedral and zoned plagioclase inclusions aligned along K-feldspar concentric bands. D) Folded magmatic foliation. Solid-state deformation is absent in these structures. E) Kfs and Crd-rich monzogranites and leucocratic veins pervading the fine-grained migmatites. Abundant K-feldspar crystals appear and are oriented around contacts and into the intrusive veins. F) Megacrystic granitoids intrude and crosscut previous migmatitic structures (isoclinal fold) but are affected by subsequent shear bands.

to monzogranitic rocks comprising one of the most abundant granitic facies in the Central System batholith, and is geochemically related to the Bt granodiorites and monzogranites of the so-called Transitional Intrusive Unit (Díaz-Alvarado *et al.*, 2011) in the Gredos massif (Fig. 3).

In order to check the geochemical composition of the experimental granodioritic glass, totally melted experiments (without solid phases) were selected to analyze the synthetic glass. A defocused beam 20mm in diameter was used for glass analyses with an electron probe microanalyser (WDS). Compositional variations have been found between the synthetic glasses (Table 1) and the SG-GEMbiot with 8 wt.% of H₂O presents a slight depletion in Na₂O and K₂O contents. However, both synthetic glasses are plotted together with the Bt granodiorites and monzogranites in geochemical diagrams representing the natural compositional variation of the granodiorites, showing similar FeO, MgO and CaO contents (Fig. 3A; B) but a higher peraluminosity for the 8 wt.% H₂O melt (Fig. 3C).

A typical Bt granodiorite sample (J707-16), far from the host-rock contacts, and a fine-grained migmatite fragment (J606-15) were used for the pelite-doped experiment (Díaz-Alvarado *et al.*, 2011) (Fig. 3; Table 1). A Bt granodiorite powder was preferred for the assimilation experiment to avoid homogenization problems when the experiment was set directly at the

final conditions and to observe the stability of K-feldspar relict crystals if these were present. Besides, J707-16 sample is included in the GEMbiot group and scarce geochemical differences are observed between the natural rock and the granodioritic synthetic glass used in the crystallization sequence simulation (SG-GEMbiot) (Fig. 3).

Experimental procedure

A granodioritic synthetic glass (Fig. 3; Table 1) was obtained homogenizing major oxides in a Carbolite furnace at temperatures around 1500°C with a standard procedure. To attain the required water-bearing compositions, a previously calculated amount of aluminum hydroxide was added and homogenized with the powder (Schmidt, 1996).

Experiments were conducted in a Boyd-England type piston-cylinder apparatus at the University of Huelva (Spain). A 12.5mm (half inch) diameter cell was used in all the experiments. Details of the design of the cell have been given by Castro *et al.* (1999, 2010). Gold capsules (3mm diameter and 0.15mm thick) were filled, sealed by pressure folding and introduced into MgO pressure containers. Temperatures were measured and controlled with Pt100-Pt87Rh13 thermocouples wired to Eurotherm 808 controllers. Oil pressures were measured with electronic DRUCK PTX 1400 pressure

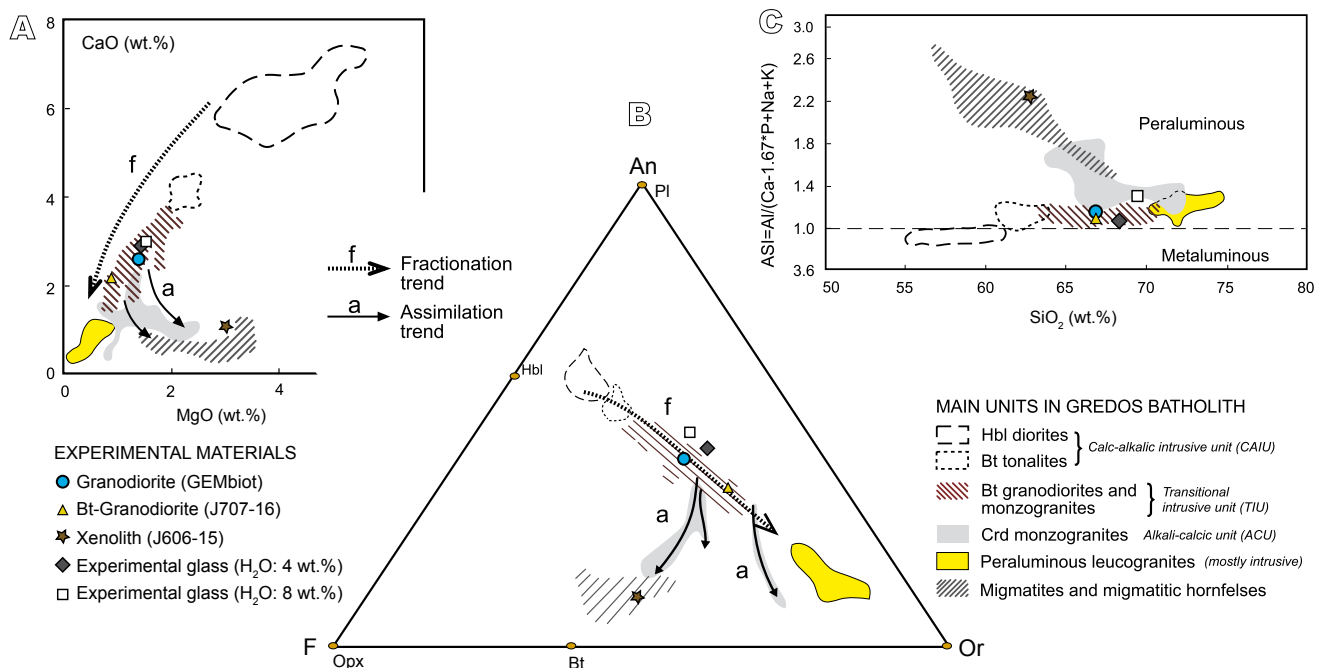


FIGURE 3. Variation diagrams showing the main geochemical characteristics of Gredos massif intrusive units (background fields) (Díaz-Alvarado *et al.*, 2011) and the starting materials used in the experimental study (Table 1). Synthetic glasses are plotted together with the Bt granodiorites and monzogranites of the Transitional Intrusive Unit (Díaz-Alvarado *et al.*, 2011). A) CaO vs. MgO diagram. B) Pseudoternary system defined by Opx-Or-An (Castro, 2013) C) ASI vs. SiO₂ granitoid classification diagram of Frost *et al.* (2001).

TABLE 1. Chemical compositions of the starting materials

Material	Ref.	SiO ₂	TiO ₂	Al ₂ O ₃	FeO _t ⁽¹⁾	MgO	MnO	CaO	Na ₂ O	K ₂ O	P ₂ O ₅	L.O.I.	Total	100-Total
Granodiorite	GEMbiot ⁽²⁾	66.87	0.55	16.29	3.62	1.40	0.05	2.57	3.30	3.95	0.29	0.71	100	
Experimental glass (H ₂ O: 4 wt.%) ⁽³⁾	SG-GEMbiot	68.32	0.51	16.60	2.35	1.47	-	2.87	3.46	4.42	-	-	100	8.59
Experimental glass (H ₂ O: 8 wt.%) ⁽³⁾	SG-GEMbiot	69.44	0.48	17.23	2.30	1.55	-	2.96	2.35	3.68	-	-	100	13.10
Bt Granodiorite ⁽⁴⁾	J707-16	66.92	0.50	15.70	3.09	0.85	0.05	2.13	3.48	4.77	0.36	1.26	99.46	
Xenolith (Fine-grained migmatite) ⁽⁴⁾	J606-15	62.81	0.86	20.00	6.26	2.98	0.08	0.68	1.68	4.64	-	-	100.0	

(1) Total iron as FeO. (2) Moreno-Ventas Bravo (1991). (3) WDS average composition. (4) Díaz-Alvarado *et al.* (2011).

transmitters, connected to OMRON E5CK controllers. Pressure was corrected manually and maintained within a narrow range of ± 0.5 MPa oil pressure, equivalent to ± 25 MPa on the sample. Heating proceeded at the maximum rate allowed by the system of 100K min^{-1} . The hot-piston-out technique was used to minimize friction effects on the pressure container (*e.g.* Johannes *et al.*, 1971).

To avoid relict phases and to achieve the total homogenization of the oxides mix in the runs, the temperature was applied in two steps, first it was set over the theoretical liquidus at the objective pressure for ≈ 30 h (*e.g.* 1050°C for 0.4GPa and $4\text{ wt.}\%$ of H_2O) and then lowered to the objective T. Run durations are specified in Table 2. All runs with two steps present minerals that were re-equilibrated at the new conditions, as demonstrated by the absence of zoning in plagioclase and the homogeneous composition of melt and minerals. A few runs were designed with intermediate steps between the maximum and the objective temperatures. In those cases, plagioclase shows concentric zoning patterns (*e.g.* GS_32, Table 2). Besides, to avoid the effects of the strong thermal gradients developed in piston-cylinder assemblies (Rodríguez *et al.*, 2015 and references therein), only the phases and compositions observed over a short distance of about 5 mm from the hotspot were taken into account.

After the desired run time, the experiments were quenched by switching the power off, which gives a cooling rate of more than 100K s^{-1} . Fast cooling is crucial to avoid the formation of quench phases. After quenching, the capsules were examined for tears and checked for proximity of the thermocouple during the run. They were cut and polished for examination by electron microprobe.

Experimental oxygen fugacity conditions are imposed by the assembly at conditions close to the quartz-fayalite-magnetite (QFM) buffer (Patiño Douce and Beard, 1996). Polished capsules were analyzed for major elements in mineral phases and glass (quenched melt) with a JEOL JXA-8200 SuperProbe at the University of Huelva. A combination of silicates and oxides were used for calibration.

In summary, 20 runs were carried out (Table 2). Eight of them (runs 1 to 8) were performed in order to constrain the liquidus surface in the granodioritic system at different pressure and H_2O conditions. A pelite-doped experiment (EA-8 Xen) simulates the interaction between the intrusive magmas and the host metapelites (Díaz-Alvarado *et al.*, 2011). The rest of them were carried out to simulate the phase relations in the high- K_2O granodioritic system at 0.4GPa with $4\text{ wt.}\%$ of H_2O .

DESCRIPTION OF THE EXPERIMENTAL RESULTS

The synthetic glass composition (SG-GEMbiot) is representative of a granodioritic to monzogranitic intrusive suite with different K-feldspar megacrystal contents, as stated before. Therefore, the results of this experimental simulation are crucial to better understand the rheological behavior of the intruding magmas and the formation of the magmatic fabrics in the Gredos massif.

Crystallization sequence

Some experiments have been conducted to test the liquidus temperatures of the synthetic glasses

TABLE 2. Experimental conditions and phase compositions

Run	Ref.	Starting material	P (GPa)	T (°C)	Duration (h) ⁽¹⁾	Water (wt.%)	
1	GS_22	SG-GEMbiot	1.0	1045	56 (2)	8	
2	GS_16	SG-GEMbiot	0.6	1012	48 (2)	8	G
3	GS_12	SG-GEMbiot	0.6	1003	49 (2)	8	G
4	GS_08	SG-GEMbiot	0.6	988	38	8	C
5	GS_14	SG-GEMbiot	0.6	1062	70 (2)	4	G
6	GS_15	SG-GEMbiot	0.6	1050	70 (2)	4	C
7	GS_11	SG-GEMbiot	0.4	1030	96	4	
8	GS_25	SG-GEMbiot	0.4	1020	55 (2)	4	

TABLE 2. (Cont.)

Run	Ref.	Starting material	P (GPa)	T (°C)	Duration (h)	Water (wt.%)	Assemblage	Phase	SiO ₂	TiO ₂	Al ₂ O ₃	FeO	MgO	MnO	CaO	Na ₂ O	K ₂ O	P ₂ O ₅	Total	100-total	An (%)				
9	GS_30	SG-GEMbiot	0.4	1010	70 (2)	4	Gl (98.7) - Mag (0.8) - Opx (0.5)	Gl	68.21	0.58	16.35	2.47	1.43	0.01	2.80	3.67	4.46	0.02	100	7.79	1.03				
								S.D.	0.26	0.04	0.12	0.22	0.10	0.01	0.05	0.07	0.01	0.29							
								Mag	1.18	3.47	4.72	80	4.88	-	0.20	0.84	0.15	-	96.26						
10	GS_33	SG-GEMbiot	0.4	980	72 (2)	4	Gl (97.1) - Mag (0.9) - Opx (2)	Gl	68.66	0.56	16.33	2.02	1.34	0.01	2.85	3.73	4.49	0.01	100	7.88	1.01				
								S.D.	0.23	0.05	0.04	0.12	0.10	0.01	0.05	0.05	0.04	0.01							
								Mag	0.41	2.30	4.03	86.06	5.49	-	0.20	-	-	100.1							
11	GS_39	SG-GEMbiot	0.4	940	48 (3)	4	Gl (95.8) - Mag (1.3) - Bt (2.9)	Gl	56.36	-	3.82	9.66	31.45	-	1.01	-	-	-	-	102.8	-	-			
								S.D.	-	-	-	-	-	-	-	-	-	-	-	-	-	-	-	-	-
								Mag	0.97	2.65	7.07	79.22	8.15	-	-	1.55	-	-	100						
12	GS_26	SG-GEMbiot	0.4	915	54 (2)	4	Gl (89.9) - Ilm (1.8) - Bt (8.3)	Gl	53.31	2.44	16.08	6.57	11.49	-	1.45	1.94	7.84	-	-	101.3	-	-			
								S.D.	70.41	0.27	16.89	1.29	0.81	0.01	3	2.99	4.31	0.02	100	8.07	1.13				
								Ilm	0.75	0.10	0.12	0.09	0.05	0.01	0.05	0.04	0.03	0.02	0.24						
13	GS_27	SG-GEMbiot	0.4	905	48 (2)	4	Gl (90) - Ilm/Mag (1.4) - Bt (7.6) - Pl (<1)	Gl	45.14	2.20	15.50	7.86	18.82	-	0.35	1.17	7.86	-	-	99.18	-	-			
								S.D.	70.73	0.29	16.91	1.32	0.64	0.01	2.94	2.86	4.29	-	100	9.04	1.15				
								Ilm	0.07	0.04	0.07	0.06	0.06	0.01	0.08	0.08	0.14	0.01	0.74						
14	GS_34 ^(B)	SG-GEMbiot	0.4	860	73 (3)	4	Gl (60) - Mag (1.7) - Bt (7.3) - Pl (31)	Gl	73.81	0.42	14.72	1.60	0.46	-	1.96	2.64	4.38	0.01	100	9.14	1.17				
								S.D.	73.81	0.42	14.72	1.60	0.46	-	1.96	2.64	4.38	0.01	100	9.14	1.17				
								Mag	1.73	0.11	1.05	0.32	0.06	-	0.33	0.20	0.05	0.02	0.55						
14	GS_34 ^(B)	SG-GEMbiot	0.4	860	73 (3)	4	Gl (60) - Mag (1.7) - Bt (7.3) - Pl (31)	Ilm	1.43	2.76	5.24	78.65	4.13	-	2.25	-	-	-	94.96	-	-				
								S.D.	10.21	13.54	3.79	62.85	1.64	-	0.31	1.15	0.71	-	95.45						
								Pl	53.09	1.85	14.58	6.50	11.56	-	1.08	1.85	6.38	-	97.09						
14	GS_34 ^(B)	SG-GEMbiot	0.4	860	73 (3)	4	Gl (60) - Mag (1.7) - Bt (7.3) - Pl (31)	Pl	60.29	-	24.55	0.74	-	8.91	5.70	0.73	-	-	100.5	61.4	-				
								S.D.	75.21	0.49	13.85	1.11	0.49	-	1.74	2.58	4.49	0.02	100	7.59	1.13				
								Mag	0.34	0.05	0.27	0.02	0.04	0.01	0.07	0.04	0.04	0.01	0.33						
14	GS_34 ^(B)	SG-GEMbiot	0.4	860	73 (3)	4	Gl (60) - Mag (1.7) - Bt (7.3) - Pl (31)	Mag	70.67	0.45	16.74	1.16	0.62	-	2.93	2.99	4.43	0.01	100	7.80	1.11				
								S.D.	0.11	0.05	0.02	0.07	0.01	-	0.04	0.04	0.02	0.01	0.18						
								Pl	0.31	1.88	2.70	84.06	5.82	-	-	-	-	-	96.23						
14	GS_34 ^(B)	SG-GEMbiot	0.4	860	73 (3)	4	Gl (60) - Mag (1.7) - Bt (7.3) - Pl (31)	Bt	54.96	3.50	15.50	6.05	9.95	-	-	-	-	-	99.50	-	-				
								S.D.	57.95	-	24.94	0.96	-	9.45	5.17	0.54	-	98.60							
								Pl	57.95	-	24.94	0.96	-	9.45	5.17	0.54	-	98.60							

TABLE 2. (Cont.)

Run	Ref.	Starting material	P (GPa)	T (°C)	Duration (h)	Water (wt.%)	Assemblage	Phase	SiO ₂	TiO ₂	Al ₂ O ₃	FeO	MgO	MnO	CaO	Na ₂ O	K ₂ O	P ₂ O ₅	Total	100- total	ASI	An (%)								
16	GS_31	SG-GEMbiot	0.4	830	97 (4)	4	G1(58.5) - Mag(0.9) - Bt(8.4) - Pl(32.2)	G1	77.43	0.37	13.67	1.01	0.25	0.02	1.52	1.62	4.10	0.02	100	11.76	1.38									
								S.D.	0.19	0.06	0.09	0.02	0.01	0.01	0.03	0.05	0.10	0.01	0.14											
								G2	72.43	0.28	16.68	1.02	0.29	0.03	2.51	2.20	4.55	0.01	100	11.17	1.27									
								S.D.	0.13	0.06	0.02	0.01	-	0.02	0.18	0.03	0.01	0.53												
								Mag	5.50	3.04	2.20	78.18	1.83	-	0.89	0.45	-	92.90												
17	GS_24	SG-GEMbiot	0.4	800	52 (2)	4	G1(55) - Mag(1.9) - Bt(9.8) - Pl(33.3)	G1	75.15	0.23	15.27	0.92	0.35	0.02	2.19	1.92	3.93	0.01	100	11.02	1.34									
								S.D.	3.95	0.07	2.10	0.23	0.28	0.02	0.80	0.53	0.54	0.01	1.80											
								Mag	-	1.30	3.14	76.34	2.02	-	2.04	0.15	-	86.04												
								Bt	41.54	2.72	13.35	9.54	13.44	-	0.31	1.07	7.10	-	89.18											
								Pl	55.91	-	21.65	0.39	-	-	6.52	5.58	1.20	-	90.54											
18	GS_35	SG-GEMbiot	0.4	750	73 (4)	4	G1(51) - Mag(2) - Bt(8.8) - Pl(38.2)	G1	82.73	0.38	12.05	0.59	0.10	0.02	1.22	0.89	2.02	0.01	100	12.35	2.05									
								S.D.	1.74	0.09	1.04	0.08	0.02	0.01	0.32	0.07	0.30	-	0.58											
								G2	71.90	0.23	16.78	0.63	0.18	0.02	3.00	2.70	4.55	0.02	100	9.73	1.13									
								S.D.	0.76	0.03	0.38	0.04	0.04	0.02	0.10	0.76	0.50	0.01	0.97											
								Mag	0.52	1.82	1.30	85.04	1.78	-	1.58	-	-	92.58												
								Bt	43.02	3.61	15.10	8.91	19.44	-	1.10	8.31	-	99.55												
								Pl	63.04	-	22.31	0.49	-	-	6.22	6.24	1.01	-	98.90											

TABLE 2. (Cont.)

Run	Ref.	Starting material	P (GPa)	T (°C)	Duration (h)	Water (wt.%)	Assemblage	Phase	SiO ₂	TiO ₂	Al ₂ O ₃	FeO	MgO	MnO	CaO	Na ₂ O	K ₂ O	P ₂ O ₅	Total	100- total	ASI	An(%)		
19	GS_32	SG-GEMbiot	0.4	700	96 (5)	4	Gl (39.5) - Ilm (1) - - Bt (7.7) - Pl (41.1) - - Kfs (10.7)	Gl S.D. Ilm Bt Pl Pl Pl Pl Kfs	79.58 1.41 24.26 50.31 53.36 58.30 61.26 65.95	0.17 0.05 9.36 2.86	12.87 0.77 3.87 14.72	0.29 0.04 58.60 7.82	0.07 0.02 0.39 11.80	0.01 0.01 -	1.29 0.32 0.38 0.77	1.62 0.17 1.03 1.12	4.09 0.80 1.14 7.61	0.01 0.02 -	100 1.15 99.06 96.87	11.36	1.36			
20	EA-8 Xen ⁽⁵⁾	J707-16 Xen (20 wt.%)	0.4	850	240	4	Gl (59), Pl (13), Qtz (7), Bt (7), Kfs (5), Crd (4), Sil (2), Spl (2), Ilm (<1), Ap (<1)	Mixed zone Gl Crd Bt Spl Kfs Xen-free zone Gl Pl Pl Pl Pl Kfs	74.48 48.02 34.48 0.89 64.37 76.81	0.21 0.01 2.94 0.27 0.02	15.06 34.11 21.04 53.64 18.75	0.90 9.49 18.28 31.68 0.12	0.27 7.40 8.96 12.77 0.02	0.04 0.40 0.14 0.02 -	0.52 0.04 0.04 0.02 0.12	2.37 0.10 0.42 0.03 2.42	6.06 0.22 9.36 0.09 13.01	0.09 -	100 99.81 95.86 99.91 99.08	4.88	1.32	8		
							(core)	62.58	-	23.20	0.13	-	-	3.86	9.03	0.24	0.02	99.13			32			
							Pl (rim)	58.20	0.06	25.79	0.29	0.02	-	7.10	6.31	1.45	0.02	99.48			52			
							Bt	41.70	3.84	17.01	9.37	15.67	0.09	0.10	0.50	8.57	0.01	97.05						
							Kfs	64.37	0.02	18.75	0.12	0.02	-	0.12	2.42	13.01	0.07	99.08						

(1) Number in brackets indicate the stages of temperature stabilization. Eg. (2) means a first stage over the liquidus temperature (1050°C at 0.4GPa) and a final stage at the objective temperature. (2) Numbers in brackets beside phases and glass are modal abundances (wt.%) measured by image analysis. Abbreviations after Kretz (1983). (3) Glass (Gl) average values in wt.% oxides for a total numbers of analyses from 4 to 10 points. Standard deviations (1 sigma) are indicated. Dashes (-) denote abundances below the detection limit. (4) Gl1 and Gl2 indicate experimental runs where two zones with different solid assemblage and glass compositions are observed. (5) Experiments from Diaz-Alvarado et al. (2011).

(SG-GEMbiot) with 4 and 8 wt.% of H₂O at different pressures (Table 2; Fig. 4). The slope of the liquidus surface for SG-GEMbiot has been determined with runs GS_22 (1.0GPa) and GS_16, GS_12 and GS_8 (0.6GPa) for H₂O contents of 8 wt.%, and runs GS_14 and GS_15 (0.6GPa) and GS_11, GS_25 and GS_30 (0.4GPa) for H₂O contents of 4 wt.% (Table 2). The SG-GEMbiot with 4 wt.% of H₂O presents few orthopyroxene crystals (0.5 vol.%) in equilibrium with the melt at 1010°C and 0.4GPa (GS_30, Table 2), and at 1050 °C and 0.6GPa (GS_15, Table 2), while the system is completely melted at 1020 (Fig. 5A) and 1062°C at 0.4 and 0.6GPa, respectively (GS_25 and GS_14, Fig. 4). Therefore, orthopyroxene is the liquidus phase in the SG-GEMbiot with 4 wt.% of H₂O between 0.4 and 0.6GPa, whereas biotite is the first crystallized phase for the synthetic glass with 8 wt.% of H₂O (Table 2; Fig. 4).

At 980°C and 4 wt.% of H₂O, run GS_33 shows magnetite and 2 vol% of orthopyroxene (Fig. 5B). Crystallization of orthopyroxene leads to a corresponding decrease in the FeO and MgO contents in the residual melt (Table 2). Lower objective temperatures (980-940°C) cause resorption of orthopyroxene and crystallization of biotite (GS_39, Table 2). Hornblende is absent in the crystallization sequence at these P-H₂O conditions. The next mineral phase that crystallizes is plagioclase at around 905°C (GS_27, Fig. 5C). Even though the presence of plagioclase is scarce in this run, at 860°C its abundance reaches 30 vol% (GS_34, Fig. 5D). Biotite

and plagioclase form the dominant solid assemblage in most of the experimental crystallization sequence. Biotite is present as fine-grained tabular crystals whereas plagioclase shows large single skeletal or hollow crystals or dendritic clusters, typical of large ΔT in the experimental procedures (Fig. 5).

Interestingly, K-feldspar is absent in runs GS_28 and GS_31, at temperatures of around 830°C (Table 2). However, the Or component in the calcic feldspar increases from 2 Or% at 860°C to 8 Or% at 830°C. This variation in the feldspar components takes place above the solvus line of the K-feldspar, which is found between 750 and 700°C in the experimental simulation results (GS_35 and GS_32, respectively, Fig. 5E; Table 2). Therefore, at 700°C the K-feldspar is present as a matrix phase. Below 700°C, only quartz crystallizes giving rise to the final mineral assemblage of plagioclase + biotite + K-feldspar + quartz \pm ilmenite \pm magnetite.

Some experiments, *e.g.* GS_31 and GS_35 (Fig. 5F), were selected to test the results of intermediate steps between the initial and the final temperatures. These experiments show two compositional zones in the capsule: in the area closer to the hotspot, the high-temperature (above 910°C) assemblage magnetite+biotite is preserved, while in the outer zone, the solid assemblage magnetite+biotite+plagioclase is in agreement with the final objective temperature of 750°C (Table 2; Fig. 5F). The contact between both zones is sharp, irregular and lobulated, and it extends across the entire capsule (Fig. 5F).

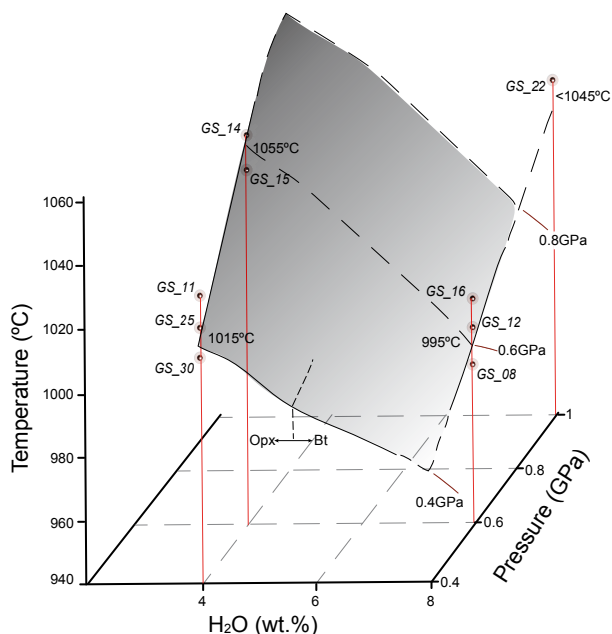


FIGURE 4. T-P-H₂O space showing the experimental liquidus surface of the high-K₂O granodioritic system. Runs that constrain the liquidus limits are indicated.

Figure 6 presents a graphical summary of the experimental crystallization sequence and the compositional evolution of the residual liquid between 1050 and 700°C for the granodioritic synthetic glass (SG-GEMbiot) with 4 wt.% of H₂O at 0.4GPa. Orthopyroxene reacts with the melt at around 940°C to form biotite, which is the liquidus phase when the initial H₂O content of the GEMbiot is above 6 wt.%. This is followed by the crystallization of plagioclase and K-feldspar at lower temperatures (Fig. 6). Quartz is the last phase that crystallizes in the analyzed high-K₂O granodioritic system.

The main changes in the composition of the liquid phase respond to the crystallization sequence. As stated above, FeO and MgO contents decrease during the crystallization of orthopyroxene (starting at 1010°C) and biotite. At temperatures around 905°C, CaO and Al₂O₃ contents suffer a marked decrease coinciding with crystallization of plagioclase. Indeed, the plagioclase composition is equilibrated with the melt at the different temperatures tested in the experiments, from 60-65 An% at 900 °C, \approx 55 An% at 830°C, and 50 An%

at 700°C (Table 2). However, the experimental run GS_32, with 3 steps during the temperature decrease, presents calcic cores (65 An%) in large plagioclase crystals (Fig.

5E), which is a common characteristic of granodioritic magmas (e.g. Castro, 2001, 2013). The K₂O content shows a small reduction at 835°C, when the Or component of

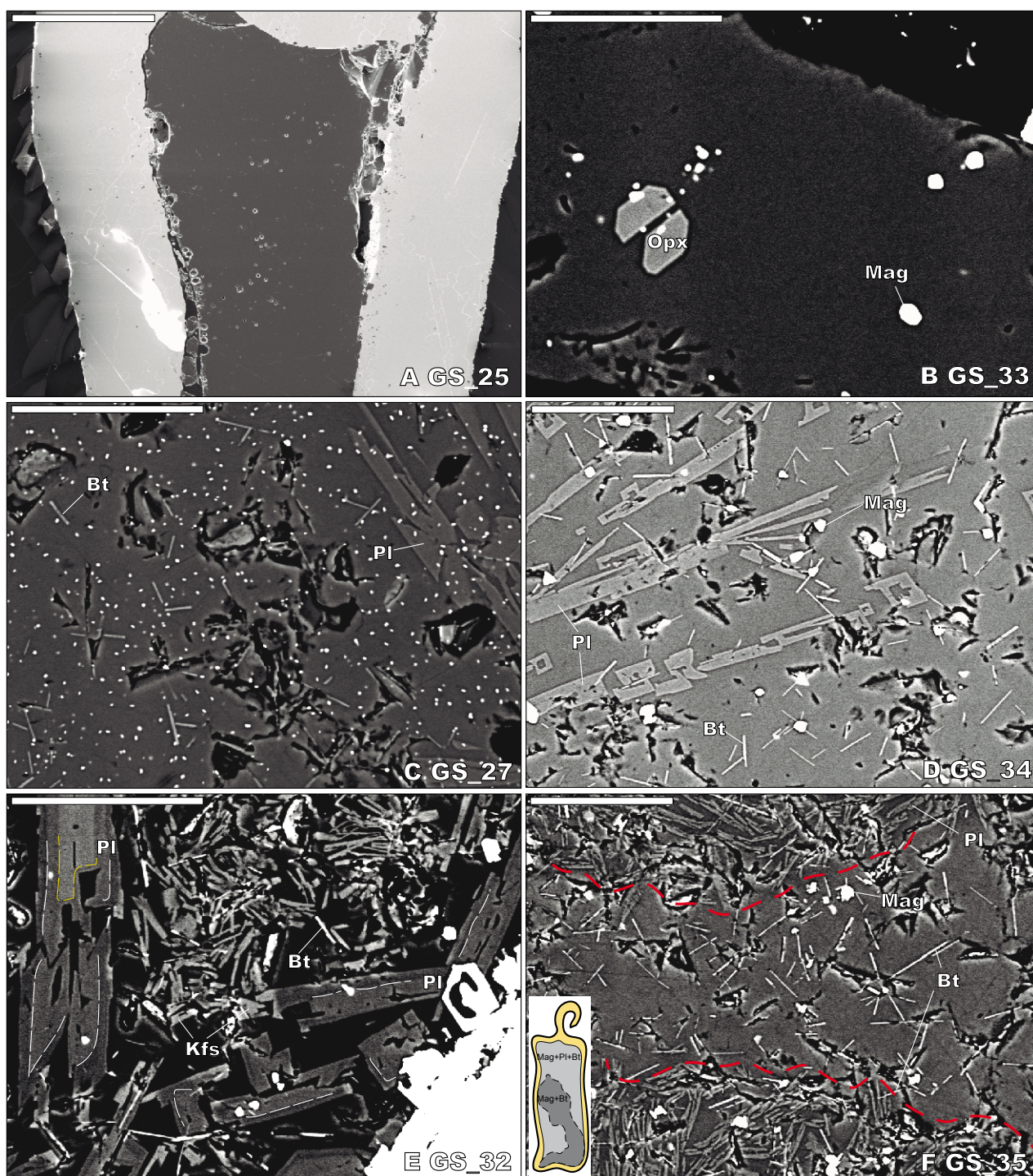


FIGURE 5. BSE images of experimental runs simulating the crystallization sequence of the K-rich granodiorites. All experiments were carried out with the synthetic glass SG-GEMbiot with 4 wt.% of H₂O at 0.4GPa and were firstly stabilized at temperatures above the liquidus (1050°C). Scale bars are 500µm for A) and 50µm for the rest of the images. A) 1020°C, the experimental capsule at temperatures above the liquidus. B) Orthopyroxene crystals at 980°C. C) and D) show the biotite+plagioclase solid assemblage at 905 and 860°C, respectively. E) K-feldspar crystallized in the matrix and large zoned plagioclase at 700°C. Dashed lines point the Ca-rich cores and rims. F) After two steps in the cooling ramp between 1050 and 750°C, two zones with different solid assemblages and glass compositions are preserved. The capsule sketch points out the arrangement of both zones.

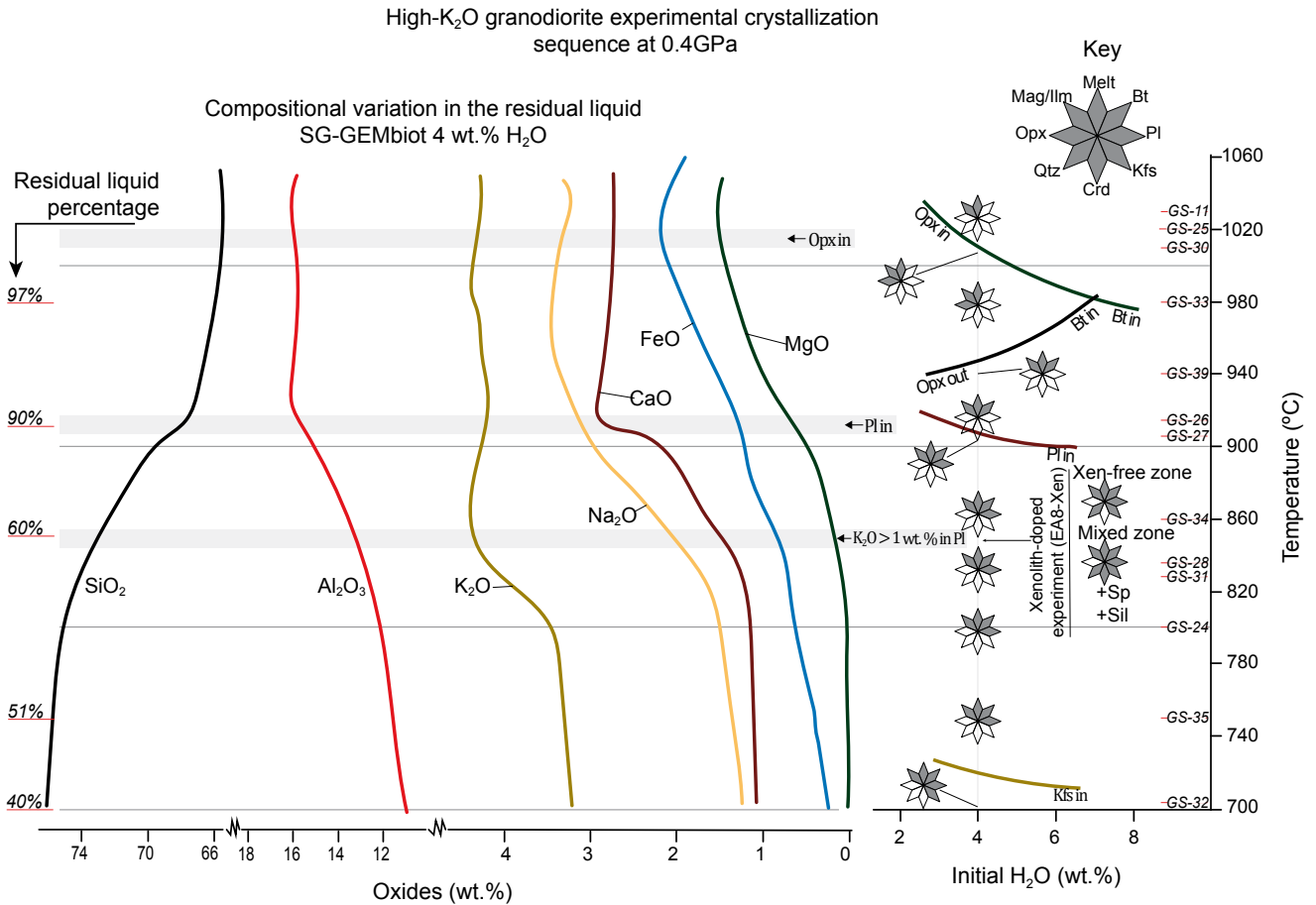


FIGURE 6. Temperature vs. initial H₂O wt.% diagram showing the graphical summary of the experimental results. Run references are indicated on the vertical axis. On the left, the compositional evolution of the melt is presented together with the liquid percentage during the crystallization sequence.

the feldspar reaches 8%. The solid assemblage reaches 60 vol% at 700°C, with 41 vol% of plagioclase, 11 vol% of K-feldspar, 8 vol% of biotite and ≈1 vol% of ilmenite (Fig. 6).

Pelitic-xenolith doped experiment

The experimental run was built by the addition of a small fragment (xenolith) of a fine-grained metapelite (J606-15) to the granodiorite powder (J-707-16) (EA8-Xen: Tables 1 and 2; Fig. 7). Experimental procedures for this experiment are detailed in Díaz-Alvarado *et al.* (2011). Experimental T and P were fixed in order to simulate the conditions (850°C and 0.4GPa) at the emplacement level in the Gredos massif (see rationale and Díaz-Alvarado *et al.*, 2011 for a discussion of these PT conditions). After a long duration of 240h, the xenolith limits were still recognizable in the capsule (Fig. 7A). Within the xenolith, a large number of phases are present: Cordierite + sillimanite + biotite + spinel + quartz + K-feldspar + Melt. Euhedral cordierite and K-feldspar crystals are clearly recognizable in this area (Fig. 7B).

In the surrounding area, the solid assemblage is similar to that of the experiment without the pelitic xenolith at the same P, T and H₂O wt.% conditions (GS_34, Fig. 5D; Table 2), except for the presence of abundant K-feldspar crystals (≈5 vol%) in the entire capsule (Fig. 7A). The composition of the melt is homogeneous across the capsule, with the only appreciable difference of the higher Al₂O₃ content within the xenoliths (15.06 and 13.58 Al₂O₃ wt.% inside and outside the xenoliths, respectively). The most significant change in the composition of the melt of this pelitic xenolith-doped experiment (EA8-Xen) compared to the melt of the granodiorite-alone run (GS_34), is a significant increase in K (5.86 and 4.49 K₂O wt.%, respectively). This phenomenon occurs in parallel with the appearance of newly-formed, euhedral K-feldspar in the composite charge at 850°C (Fig. 7A).

DISCUSSION

This work shows the results of the experimental simulation of the crystallization sequence in a

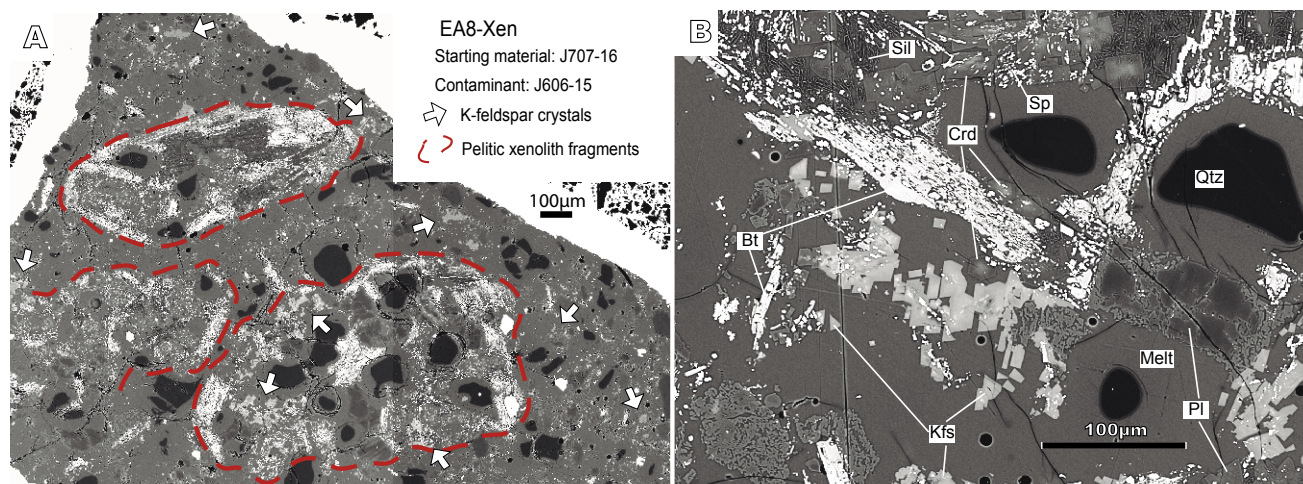


FIGURE 7. BSE images of an experimental run simulating the interaction between Bt granodiorite and fragments of pelitic xenoliths. Scale bars are 100 μ m. A) General aspect of the experimental capsule showing the xenolith boundaries. White arrows mark some of the K-feldspar crystals inside and outside the xenolith areas. B) Textures and mineral phases in the xenolith boundaries. Euhedral cordierite and K-feldspar crystallize in the capsule in contrast to that observed in the granodiorite-alone run at 860°C (GS_34, Fig. 5), but only K-feldspar crystals appear out of the xenolith domain.

granodioritic composition and the interaction between the granodioritic to monzogranitic melts and the pelitic host rocks at the emplacement P-H₂O conditions of the Gredos massif. The K₂O content of the intrusive magmas and the geochemical contribution of the host metapelites are pointed as the key factors for the early crystallization of large euhedral K-feldspar crystals, which are not depicted in previous experimental studies of megacrystic granites and in the phase relations presented above in the experiments without pelite fragments.

Experimental simulation of the phase relations in the K-rich granodioritic system

Liquidus temperatures increase with pressure and decrease with the H₂O content (Fig. 4), which is coincident with the results observed in the T vs. H₂O content diagrams at 0.2 and 0.8GPa of Naney (1983). The liquidus temperature of the high-K₂O granodioritic composition (SG-GEMbiot) is around 1015°C at 0.4GPa and 4 wt.% of H₂O (Fig. 4; Table 2). This result is approximately coincident with the liquidus temperature obtained for granodioritic compositions by Naney (1983), calculated by extrapolating data from 0.2 and 0.8GPa. Bogaerts *et al.* (2006) present slightly higher liquidus temperatures for a granodioritic system with SiO₂ contents similar to those of the GEMbiot, albeit it is substantially richer in FeO, MgO and CaO. Therefore, on account of the similarities found in these experimental studies, the results obtained in the Bt granodiorites of the Central System batholith are, thus, representative of most of the (porphyritic) granodiorites.

The crystallization sequence obtained from the experimental simulation with the SG-GEMbiot with 4 wt.% of H₂O at 0.4GPa shows orthopyroxene as the liquidus phase at 1010°C (Figs. 5B and 6). Between 980 and 940°C, the orthopyroxene is replaced by biotite through the reaction orthopyroxene+liquid=biotite. The calcic plagioclase (>60An%) liquidus line is found around 900°C, while the crystallization of the K-feldspar is comprised between 750 and 700°C in the SG-GEMbiot (Fig. 6; Table 2). Therefore, at 700°C the experimental capsule is composed by plagioclase (41%), K-feldspar (11%), biotite (8%), magnetite (\approx 1%) and glass (39%) (Fig. 8). However, at 850°C, the K-feldspar is absent, in contrast with the 5 vol% of euhedral K-feldspar found in the pelite-doped experiment (Figs. 7 and 8). Finally, at lower temperatures quartz is expected to crystallize completing the typical solid assemblage of Bt granodiorites and monzogranites.

The hornblende is absent in both the natural rocks and the experimental mineral assemblage of the GEMbiot granodiorites. This suggests that the stability field of Hbl depends not only on the pressure and water conditions, but also on the small compositional differences between the starting materials (Naney, 1983). Hornblende is stable for H₂O contents above 5.3 wt.% and at 0.4GPa in the experiments of Bogaerts *et al.* (2006), contrary to what is observed in the experiments for a granodiorite system poorer in FeO, MgO and CaO, where biotite is the stable phase at high H₂O contents (Fig. 4).

The presence of zones with different mineral assemblages in the experimental capsules (Fig. 5F) when the cooling ramp is stepped is a result of the thermal

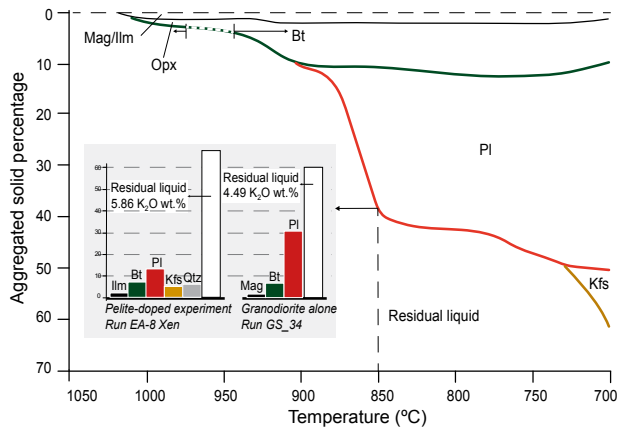


FIGURE 8. Aggregated solid percentage vs. temperature diagram representing the evolution of the mineral assemblage in the experimental simulation of the crystallization sequence. The histograms of the inset points the increase of the K_2O content in the residual liquid and the early crystallization of K-feldspar as the most outstanding characteristics of the pelite-doped experiment (EA-8 Xen) regarding to the granodiorite-alone run (GS_34) at 850°C and 0.4GPa.

gradients caused in the experimental assemblages. The domains with high-temperature assemblages are preserved at lower temperatures, therefore coexisting the magnetite+biotite high-temperature assemblage and the magnetite+biotite+plagioclase low-temperature assemblage in run GS_35 (Fig. 5F; Table 2). Similar variations in mineral composition and abundances between granitic facies are often observed in batholiths and are related to the complexity of cooling and crystallization processes in magma chambers and conduits (Rodríguez *et al.*, 2015; Rodríguez and Castro, 2017).

The early or late crystallization of K-feldspar in megacrystic granites

In the experimental results shown in this work, crystallization of K-feldspar is limited between 750 and 700°C (Figs. 6 and 8). These results imply that the textural domain of the K-feldspar in the GEMbiot granodiorite suite is restricted to the matrix. Other experimental simulations where K-feldspar crystallization temperatures are close to the solidus of the granodioritic system (*e.g.* Piwinski, 1968; Johnson and Rutherford, 1989) coincide with the results presented in this work. According to field evidences in the Gredos massif (Fig. 2), the textural relations of the K-feldspar megacrysts with the rest of mineral phases is equivalent to that of phenocrysts relative to their matrix. However, the crystallization sequence obtained here from the SG-GEMbiot runs discards an early growth of K-feldspar crystals. If these K-feldspar megacrysts were incidentally included by any process in the SG-GEMbiot system at temperatures close to its liquidus, a remarkable

textural disequilibrium of these megacrysts is expected to occur, generating resorption surfaces and other textural features that should be easily recognized in the field. Therefore, the presence of K-feldspar megacrysts in granodioritic rocks, in apparent textural equilibrium with their matrix, suggests that: i) K-feldspar crystals grow to large grain sizes below nominal solidus temperatures (Glazner and Johnson, 2013) or ii) other magmatic processes, like assimilation or hybridization, operated during the crystallization of the Bt granodiorites and monzogranites in the Gredos massif. Textural evidences as euhedral shape, megacrystic size or plagioclase and biotite inclusion alignment, and structural characteristics as magmatic foliations, K-feldspar crystals oriented around magma-magma and magma-host rock contacts, K-feldspar abundance variations in magmatic facies and the absence of solid-state structures or plastically deformed K-feldspar megacrysts (Fig. 2) are not in agreement with a sub-solidus megacrystic growth of K-feldspar. Therefore, the early K-feldspar crystallization triggered by the interaction process between a granodioritic magma and the host metasediments has been assessed through a pelite-doped experiment.

The pelite-doped experiment shows that the interaction of the granodioritic liquid with pelitic xenoliths promotes crystallization of euhedral Crd in the reactive area of the xenolith and euhedral K-feldspar crystals in the entire experimental capsule (Fig. 7). Interestingly, the melt fraction across the capsule shows a highly homogeneous composition attaining 5.86 wt.% of K_2O (EA-8 Xen, Table 2). Whole rock compositions of granodiorites and monzogranites along the Central System batholith show K_2O contents between 3.5 and 7 wt.% (*e.g.* Moreno-Ventas Bravo, 1991; Díaz-Alvarado *et al.*, 2011) and K-feldspar megacryst percentages vary from <10 to >25%, showing the higher abundances close to the metasedimentary host-rocks (Fig. 1D). Based on the mineral abundances and the melt K_2O content found in the pelite-doped experiment (Table 2), Table 3 presents the estimations of the K-feldspar abundance according to the volume of assimilated material described in the granodiorites and monzogranites of the Gredos massif (Ugidos *et al.*, 2008; Díaz-Alvarado *et al.*, 2011). Values of 7 wt.% K_2O in the granodioritic magmas involve K-feldspar abundances up to 15-20 vol%, which are frequently observed in the Gredos massif (Fig. 2), mostly close to the host-rock contacts. Moreover, this process also causes the crystallization of K-feldspar at higher temperatures than those predicted by the experimental simulation of the crystallization sequence in the SG-GEMbiot (Fig. 8), thereby casting some light upon the problem of the relatively early growth and large grain-size of these K-feldspar megacrysts (Fig. 9). Geochemical zonation and successive crystal growth

TABLE 3. Projections of the mineral abundances in the granodiorites and monzogranites according to the extent of the assimilation process

Assimilation (%)	Reference experiment	Initial bulk K ₂ O (wt.%)	Melt K ₂ O (wt.%) at 850 °C	Kfs abundance (vol.%)	Crd abundance (vol.%)
0	GS_34 ⁽¹⁾	4.42	4.49	0	0
20	EAB-Xen ⁽²⁾	4.77	5.86	5-8	4
50	Projection	4.77	7.5	12.5-20	10

(1) Starting granodioritic material : SG-GEMbiot with 4 wt.% of H₂O (Table 1).

(2) Starting granodioritic material: J707-16 (Table 1).

stages were favored by the intrusion of new magma and H₂O and K₂O-rich fluids released during the melting process in migmatitic host-rocks. Besides, this process involves a slow cooling rate that promoted a growing rate vs. nucleation ratio high enough to form large crystals.

The crystallization of K-feldspar megacrysts at the emplacement level following the interaction of a granodiorite magma with its host metasediments may explain the absence of megacrysts in volcanic rocks of granodioritic composition. Volcanic textures in this case are the result of rapid magma ascent and crystallization processes, which impedes geochemical interaction with host crustal rocks. Therefore, this type of volcanic rocks shows normal phase relations, as those described in the experimental simulations with SG-GEMbiot.

The significance of the foliations defined by K-feldspar megacrysts as magmatic fabrics

Evidences favoring an early crystallization of K-feldspar megacrysts under some circumstances confirm that their fabrics, observed in many granitic plutons, are magmatic in origin. These fabrics are commonly the result of the interaction between internal (magmatic) and external (tectonic) kinematic processes during the evolution of magma (*e.g.* Mulchrone *et al.*, 2005). These processes comprise those due to the ascent, emplacement, cooling and thermal rejuvenation of magmas, including the effects of magmatic inputs and reactivation of magmatic structures (Kratinová *et al.*, 2007; Zák *et al.*, 2007). Magmatic fabrics are formed largely by rotation of rigid particles in a viscous environment and, accordingly, they should be relatively early features (crystallinities < 50 vol%) relative to the crystallization history (Mulchrone *et al.*, 2005). However, the strain increments related to the final stages of crystallization also may play a significant role in the final appearance of magmatic fabrics (Paterson *et al.*, 1998).

The anisotropy observed in megacrystic granites is mainly marked by the preferred orientation of K-feldspar megacrysts. Magmatic foliations point to an early origin

for this phase. According to the experimental results presented here, K-feldspar crystallization occurs at the emplacement level, where the interaction with the pelitic host rocks is possible, triggered by the increase in the K₂O wt.% of the granodioritic magmas. This promotes an important rise in the crystal fraction and the change in the rheological state of the intrusive magmas.

In the Gredos massif, magmatic fabrics with both flattening and constrictional shape ellipsoids, the latter probably related to magma flow during its ascent and emplacement, are preserved (Díaz-Alvarado *et al.*, 2012). However, magmatic structures were indirectly induced by regional deformation that conditioned the shape and orientation of the ascent conduits and emplacement structures. Also, previous fabrics were overprinted by displacement along sub-horizontal extensional shear zones, and by the effects of vertical shortening due to the overburden weight (Díaz-Alvarado *et al.*, 2012). Accordingly, the magmatic foliation observed in the granitoids and the migmatitic foliation of host-rocks are sub-parallel (Figs. 1B and 2). The shear zones controlling the emplacement of the granodiorite magma batches profited from the weakness surfaces defined by the foliation in the host rocks, thereby explaining the parallelism of the fabric described above. Therefore, the magmatic and migmatitic fabrics share the same kinematic information favored by the low viscosity difference between the migmatitic metasediments and the partially crystallized (K-feldspar-rich) magmas.

Tectonic setting and petrogenesis of the late Carboniferous megacrystic granites of the Central System batholith

The Central System batholith represents one of the most voluminous granitic exposures of late Carboniferous to early Permian ages. Most of them share calc-alkaline characteristics and other subduction-related geochemical signatures typical of cordilleran batholiths (Castro *et al.*, 2002; Díaz-Alvarado *et al.*, 2011; Pereira *et al.*, 2015). This magmatism has been recently related to the subduction of the Paleotethys oceanic plate in the core of Pangaea, a tectonic scenario that is configured late regarding to the Variscan orogeny (*ca.* 360Ma) (Pereira *et al.*, 2015).

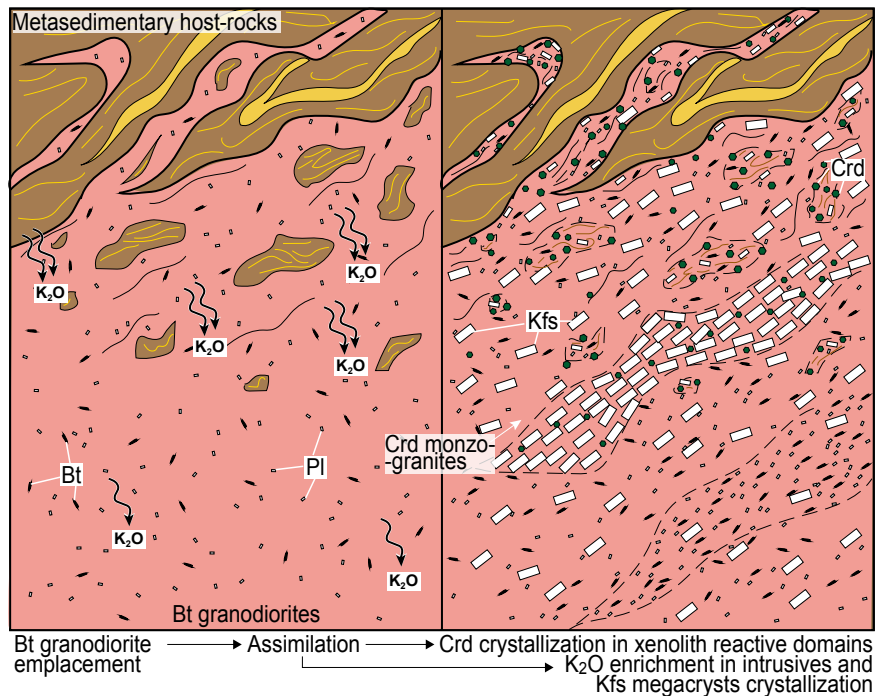


FIGURE 9. Schematic model of emplacement and interaction of granodioritic magma batches and metasedimentary host rocks at the migmatitic middle crust.

This experimental study shows how the mineralogical and geochemical characteristics of pristine calc-alkaline magmas are modified at the emplacement level by interaction with the metasedimentary host rocks. Assimilation of pelitic xenoliths promotes short range local equilibrium and cordierite crystallization and more effective distribution and homogenization of K_2O -rich fluids that trigger the early K-feldspar crystallization and the characteristically porphyritic textures observed in the Central System batholith.

CONCLUSIONS

The changes observed in the mineral assemblages and the melt compositions of the granodioritic systems in the Central System batholith, Iberian Massif, in presence of pelitic metasediments suggest that K-feldspar megacrysts are the result of the migration of H_2O and K_2O -rich fluids released during the assimilation of the partially melted pelitic host-rocks into the intrusive magmas, which are effectively homogenized in the granodioritic melt, promoting the early euhedral crystallization of large K-feldspar. This is in agreement with most of the geochemical, petrographic and textural characteristics described in the megacrystic granites.

According to the experimental results, the granodioritic magma probably intruded the emplacement level at

temperatures above $900^\circ C$ with a low crystal fraction (<20-30% crystals) and a solid assemblage of plagioclase+biotite. Afterwards, the interaction between the metasedimentary host-rocks and the granodioritic magma promoted the early crystallization of K-feldspar, which agrees with the growth of large euhedral K-feldspar crystals with aligned plagioclase and biotite inclusions. The crystal growth to megacrystic sizes may be explained by the incremental and sequential magmatic input that maintains the temperatures above the solidus in the granodioritic system. The long duration of the emplacement and cooling processes in the Gredos massif favored the geochemical homogenization of magmas and the pervasive flow of K_2O -rich fluids along the entire batholith.

ACKNOWLEDGMENTS

I acknowledge Antonio Castro for introducing me to the fascinating world of the experimental petrology. I am grateful to Carlos Fernández, Antonio Castro and Ignacio Moreno-Ventas for their support and tenacious advice during my PhD studies. Also, I would like to thank Guillermo Corretgé for his excellent contribution to the Earth Sciences in Spain and the guidance of this experimental work.

This paper was part of the PhD studies of J. Díaz-Alvarado, carried out at the Experimental Petrology Unit of the CSIC-University of Huelva, and the Departments of Geology and

Geodynamics and Palaeontology, University of Huelva, with a Grant Fellowship from the Spanish Ministry of Science and Innovation (Grant no. AP2005-3489). The project was also funded with the Grants CGL2004-06808-CO4-01/BTE, CGL2004-06808-CO4-02/BTE and CGL2007-63237/BTE of the Spanish Ministry of Science and Innovation.

REFERENCES

- Boettcher, A.L., Wyllie, P.J., 1969. Phase relationships in the system $\text{NaAlSi}_3\text{O}_8\text{-SiO}_2\text{-H}_2\text{O}$ to 35 kilobars pressure. *American Journal of Science*, 267, 875-909.
- Bogaerts, M., Scaillet, B., Vander Auwera, J., 2006. Phase equilibria of the Lyngdal Granodiorite (Norway): Implications for the origin of meta-aluminous ferroan granitoids. *Journal of Petrology*, 47(12), 2405-2431.
- Burnham, C.W., 1979. The importance of volatile constituents. In: Yoder, H.S.J. (ed.). *The Evolution of the Igneous Rocks*. Princeton, New Jersey, Princeton University Press, 602pp.
- Burnham, C.W., Wayne, C., Jahns, R.H., 1962. A method for determining the solubility of water in silicate melts. *American Journal of Science*, 260, 721-745.
- Capdevila, R., Corretgé, L.G., Floor, P., 1973. Les granitoides varisques de la Mesete Iberique. *Bulletin de la Société Géologique de France*, 7-15, 209-228.
- Castro, A., 2001. Plagioclase morphologies in assimilation experiments. Implications for disequilibrium melting in the generation of granodiorite rocks. *Mineralogy and Petrology*, 71, 31-49.
- Castro, A., 2013. Tonalite-granodiorite suites as cotectic systems: a review of experimental studies with applications to granitoid petrogenesis. *Earth Science Reviews*, 124, 68-95.
- Castro, A., Patiño Douce, A., Corretgé, L.G., de la Rosa, J.D., El-Blad, M., El-Hmidi, H., 1999. Origin of peraluminous granites and granodiorites, Iberian Massif, Spain: an experimental test of granite petrogenesis. *Contributions to Mineralogy and Petrology*, 135, 255-276.
- Castro, A., Corretgé, L.G., de la Rosa, J., Enrique, P., Martínez, F.J., Pascual, E., Lago, M., Arranz, E., Galé, C., Fernández, C., Donaire, T., López, S., 2002. Paleozoic magmatism. In: Gibbons, W., Moreno, M.T. (eds.). *The Geology of Spain*. Geological Society, London, 117-153.
- Castro, A., García Casco, A., Fernández, C., Corretgé, L.G., Moreno-Ventas, I., Gerya, T., Löw, I., 2009. Ordovician ferrosilicic magmas: experimental evidence for ultrahigh temperatures affecting a metagreywacke source. *Gondwana Research*, 16, 622-632.
- Castro, A., Gerya, T., García-Casco, A., Fernández, C., Díaz-Alvarado, J., Moreno-Ventas, I., Löw, I., 2010. Melting relations of MORB-sediment mélanges in underplated mantle wedge plumes; implications for the origin of Cordilleran-type batholiths. *Journal of Petrology*, 51, 1267-1295.
- Díaz Alvarado, J., Castro, A., Fernández, C., Moreno-Ventas, I., 2011. Assessing bulk assimilation in cordierite-bearing granitoids from the central system batholith, Spain; experimental, geochemical and geochronological constraints. *Journal of Petrology*, 52, 223-256.
- Díaz Alvarado, J., Fernández, C., Díaz Azpiroz, M., Castro, A., Moreno-Ventas, I., 2012. Fabric evidence for granodiorite emplacement with extensional shear zones in the Variscan Gredos massif (Spanish Central System). *Journal of Structural Geology*, 42, 74-90.
- Díaz-Alvarado, J., Castro, A., Fernández, C., Moreno-Ventas, I., 2013. SHRIMP U-Pb zircon geochronology and thermal modeling of multilayer granitoid intrusions. Implications for the building and thermal evolution of the central system batholith, Iberian Massif, Spain. *Lithos*, 175-176, 104-123.
- Díaz-Alvarado, J., Fernández, C., Chichorro, M., Castro, A., Pereira, M.F., 2016. Tracing the Cambro-Ordovician ferrosilicic to calc-alkaline magmatic association in Iberia by in situ U-Pb SHRIMP zircon geochronology (Gredos massif, Spanish Central System batholith). *Tectonophysics*, 681, 95-110.
- Farina, F., Dini, A., Innocenti, F., Rocchi, S., Westerman, D.S., 2010. Rapid incremental assembly of the Monte Capanne pluton (Elba Island, Tuscany) by downward stacking of magma sheets. *Geological Society of America Bulletin*, 122, 1463-1479.
- Farina, F., Stevens, G., Villaros, A., 2012. Multi-batch, incremental assembly of a dynamic magma chamber: the case of the Peninsula pluton granite (Cape Granite Suite, South Africa). *Mineralogy and Petrology*, 106(3), 193-216.
- Fernández, C., Becchio, R., Castro, A., Viramonte, J.M., Moreno-Ventas, I., Corretgé, L.G., 2008. Massive generation of atypical ferrosilicic magmas along the Gondwana active margin: implications for cold plumes and back-arc magma generation. *Gondwana Research*, 14, 451-473.
- Frost, B.R., Barnes, C.G., Collins, W.J., Arculus, R.J., Ellis, D.J., Frost, C.D., 2001. A geochemical classification for granitic rocks. *Journal of Petrology*, 42, 2033-2048.
- García-Arias, M., Stevens, G., 2017. Phase equilibrium modelling of granite magma petrogenesis: B. An evaluation of the magma compositions that result from fractional crystallization. *Lithos*, 277, 109-130.
- Glazner, A.F., Johnson, B.R., 2013. Late crystallization of K-feldspar and the paradox of megacrystic granites. *Contributions to Mineralogy and Petrology*, 166, 777-799.
- Holtz, F., Becker, A., Freise, M., Johannes, W., 2001. The water-undersaturated and dry Qz-Ab-Or system revisited. Experimental results at very low water activities and geological implications. *Contributions to Mineralogy and Petrology*, 141, 347-357.
- James, R.S., Hamilton, D.L., 1969. Phase relations in the system $\text{NaAlSi}_3\text{O}_8\text{-KAlSi}_3\text{O}_8\text{-CaAlSi}_2\text{O}_8\text{-SiO}_2$ at 1kbar water pressure. *Contributions to Mineralogy and Petrology*, 21, 111-141.

- Johannes, W., Holtz, F., 1996. *Petrogenesis and Experimental Petrology of Granitic Rocks*. Springer, Berlin Heidelberg, 335pp.
- Johannes W., Chipman, D.W., F, H.J., Bell, P.M., Mao, H.K., Newton, R.C., Boettcher, A.L., Seifert, F., 1971. An interlaboratory comparison of piston-cylinder pressure calibration using the albite-breakdown reaction. *Contributions to Mineralogy and Petrology*, 32, 24-38
- Johnson, M.C., Rutherford, M.J., 1989. Experimentally determined conditions in the Fish Canyon Tuff, Colorado, magma chamber. *Journal of Petrology*, 30, 711-737.
- Johnson, B.R., Glazner, A.F., 2010. Formation of K-feldspar megacrysts in granodioritic plutons by thermal cycling and late-stage textural coarsening. *Contributions to Mineralogy and Petrology*, 159, 599-619.
- Kim, K.T., Burley, B.J., 1971. Phase Equilibria in the System $\text{NaAlSi}_3\text{O}_8$ - NaAlSiO_4 - H_2O with Special Emphasis on the Stability of Analcite. *Canadian Journal of Earth Sciences*, 8, 311-337.
- Kratinová, Z., Schulmann, K., Edel, J.B., Jezek, J., Schaltegger, U., 2007. Model of successive granite sheet emplacement in transtensional setting: integrated microstructural and anisotropy of magnetic susceptibility study. *Tectonics*, 26, TC6003. DOI: 10.1029/2006TC002035.
- Lambert, I.B., Robertson, J.K., Wyllie, P.J., 1969. Melting reactions in the system KAlSi_3O_8 - SiO_2 - H_2O to 18.5 kilobars. *American Journal of Science*, 267, 609-626.
- Lindsley, D.H., 1967. P-T projection for part of the system kalsitesilica. *Carnegie Institution Washington Yearbook*, 65, 244-247.
- London, D., 2009. The origin of primary textures in granitic pegmatites. *The Canadian Mineralogist*, 47, 697-724.
- Luth, R.W., 1969. The systems $\text{NaAlSi}_3\text{O}_8$ - SiO_2 and KAlSi_3O_8 - SiO_2 to 20kb and the relationship between H_2O content, PH_2O , and P_{total} in granitic magmas. *American Journal of Science*, 267-A, 325-341.
- Luth, R.W., 1976. *Granitic Rocks*. In: Balley, D.K., Mac Donald, R., (eds.). *The Evolution of the Crystalline Rocks*, Academic Press, London, 335-417.
- Luth, R.W., Jahns, R.H., Tuttle, O.F., 1964. The granite system at pressures of 4 to 10 kilobars. *Journal of Geophysical Research*, 69, 759-773.
- Maaløe, S., Wyllie, P.J., 1975. Water content of a granite magma deduced from the sequence of crystallization determined experimentally with water-undersaturated conditions. *Contributions to Mineralogy and Petrology*, 52, 175-191.
- Merril, R.B., Robertson, J.K., Wyllie, P.J., 1970. Melting reactions in the system $\text{NaAlSi}_3\text{O}_8$ - KAlSi_3O_8 - SiO_2 - H_2O to 20 kilobars compared with results for other feldspar-quartz- H_2O and rock- H_2O systems. *Journal of Geology*, 78, 558-569.
- Moore, J.G., Sisson, T.W., 2008. Igneous phenocrystic origin of K-feldspar megacrysts in granitic rocks from the Sierra Nevada batholith. *Geosphere*, 4, 387-400.
- Moreno-Ventas, I., 1991. *Petrología de los Granitoides y Rocas Básicas asociadas de la Sierra de Gredos, Sistema Central Español*. PhD Thesis, Huelva, Universidad de Sevilla, 431pp.
- Moreno-Ventas, I., Rogers, G., Castro, A., 1995. The role of hybridization in the genesis of Hercynian granitoids in the Gredos massif, Spain: inferences from Sr-Nd isotopes. *Contributions to Mineralogy and Petrology*, 120, 137-149.
- Mulchrone, K.F., Grogan, S., De, P., 2005. The relationship between magmatic tilting, fluid flow and crystal fraction. *Journal of Structural Geology*, 27, 179-197.
- Naney, M.T., 1983. Phase equilibria of rock-forming ferromagnesian silicates in granitic systems. *American Journal of Science*, 283, 993-1033.
- Parga-Pondal, I., Matte, P., Capdevila, R., 1964. Introduction à la géologie de l'Ollo de Sapo, formation porphyroïde anté-silurienne du Nord-Ouest de l'Espagne. *Notas y Comunicaciones del Instituto Geológico y Minero de España*, 76, 119-153.
- Paterson, S.R., Fowler, T.K., Schmidt, K.G., Yoshinobu, A.S., Yuan, E.S., Miller, R.B., 1998. Interpreting magmatic fabric patterns in plutons. *Lithos*, 44, 53-82.
- Patiño Douce, A.E., 1996. Effects of pressure and H_2O content on the compositions of primary crustal melts. *Transactions of the Royal Society of Edinburgh, Earth Science*, 87, 11-21.
- Patiño Douce, A.E., Beard, J.S., 1996. Effects of P , $f(\text{O}_2)$ and Mg/Fe ratio on dehydration-melting of model metagreywackes. *Journal of Petrology*, 37, 999-1024.
- Pereira, M.F., Castro, A., Fernández, C., 2015. The inception of a Paleotethyan magmatic arc in Iberia. *Geoscience Frontiers*, 6, 297-306.
- Peters, T., Luth, R.W., Tuttle, O.F., 1966. The melting of analcite solid solutions in the system NaAlSiO_4 - $\text{NaAlSi}_3\text{O}_8$ - H_2O . *American Mineralogist*, 51, 736-753.
- Piwinskii, A.J., 1968. *Studies of batholithic feldspars: Sierra Nevada, California*. *Contributions to Mineralogy and Petrology*, 17, 204-223.
- Piwinskii, A.J., Wyllie, P.J., 1968. Experimental studies of igneous rock series: A zoned pluton in the Willowa batholith, Oregon. *Journal of Geology*, 76, 205-234.
- Piwinskii, A.J., Wyllie, P.J., 1970. Experimental studies of igneous rock series: Felsic body suite from Needle Point pluton, Willowa batholith, Oregon. *Journal of Geology*, 78, 52-76.
- Rodríguez, C., Castro, A., 2017. Silicic magma differentiation in ascent conduits. *Experimental constraints*. *Lithos*, 272-273, 261-277.
- Rodríguez, C., Geyer, A., Castro, A., Villaseñor, A., 2015. Natural equivalents of thermal gradient experiments. *Journal of Volcanology and Geothermal Research*, 298, 47-58.
- Rodríguez Alonso, M.D., Díez Balda, M.A., Perejón, A., Pieren, A., Liñán, E., López Díaz, F., Moreno, F., Gámez Vintaned, J.A., González Lodeiro, F., Martínez Poyatos, D., Vegas, R., 2004. *Dominio del Complejo Esquisto-grauváquico. Estratigrafía. La secuencia litoestratigráfica del Neoproterozoico-Cámbrico Inferior*. In: Vera, J.A., (ed.). *Geología de España*. Sociedad Geológica Española (SGE)-Instituto Geológico y Minero de España (IGME), Madrid, 78-81.
- Scarfe, C.M., Luth, R.W., Tuttle, O.F., 1966. An experimental study bearing on the absence of leucite in plutonic rocks. *American Mineralogist*, 51, 726-735.

- Schmidt, M.W., 1996. Experimental constraints on recycling of potassium from subducted oceanic crust. *Science*, 272, 1927-1930.
- Steiner, J.C., 1970. An experimental study of the assemblage alkali feldspar + liquid + quartz in the system NaAlSi₃O₈-KAlSi₃O₈-SiO₂-H₂O at 4000bars. PhD Thesis, Stanford University, 98pp.
- Steiner, J.C., Jahns, R.H., Luth, R.W., 1975. Crystallization of alkali feldspar and quartz in the haplogranite system NaAlSi₃O₈-KAlSi₃O₈-SiO₂-H₂O at 4kbar. *Geological Society of America Bulletin*, 86, 83-97.
- Thomas, R., 2000. Estimation of water contents of granite melt inclusions by confocal laser Raman microprobe spectroscopy. *American Mineralogist*, 85, 868-872.
- Tuttle, O.F., Bowen, N.L., 1958. Origin of granite in the light of experimental studies in the system NaAlSi₃O₈-KAlSi₃O₈-SiO₂-H₂O. *The Geological Society of America Memoir*, 74, 1-146.
- Ugidos, J.M., Stephens, W.E., Carnicero, A., Ellam, R.M., 2008. A reactive assimilation model for regional-scale cordierite-bearing granitoids: geochemical evidence from the Late Variscan granites of the Central Iberian Zone, Spain. *Earth and Environmental Science Transactions of the Royal Society of Edinburgh*, 99, 225-250.
- Vernon, R.H., Paterson, S.R., 2008. How late are K-feldspar megacrysts in granites? *Lithos*, 104, 327-336.
- Vignerresse, J.L., 2014. Textures and melt-crystal-gas interactions in granites. *Geoscience Frontiers*, 6, 635-663.
- Weinberg, R.F., Sial, A.N., Pessoa, R.R., 2001. Magma flow within the Tavares pluton, northeastern Brazil: compositional and thermal convection. *Bulletin of the Geological Society of America*, 113, 508-520.
- Whitney, J.A., 1975. The effects of pressure, temperature, and XH₂O on phase assemblage in four synthetic rock compositions. *Journal of Geology*, 83, 1-31.
- Whitney, J.A., 1988. The origin of granite; the role and source of water in the evolution of granitic magmas. *Geological Society of America Bulletin*, 100, 1886-1897.
- Wyllie, P.J., 1979. Magmas and volatile components. *American Journal of Science*, 64, 469-500.
- Zák, J., Paterson, S.R., Memeti, V., 2007. Four magmatic fabrics in the Tuolumne batholith, central Sierra Nevada, California (USA): implications for interpreting fabric patterns in plutons and evolution of magma chambers in the upper crust. *Geological Society of America Bulletin*, 119, 184-201.

Manuscript received March 2017

revision accepted June 2017;

published Online October 2017.